The Astrophysical Journal, 671:912–925, 2007 December 10

THE PHYSICAL PROPERTIES OF CORONAL STREAMERS. II.

M. Uzzo,[1] L. Strachan,[1] and A. Vourlidas[2]
Received 2006 December 6; accepted 2007 August 19

ABSTRACT

In this paper the plasma properties of three streamers observed in 2003 by the Ultraviolet Coronagraph Spectrometer (UVCS) are presented for five heights from 1.75 to 5.0 $R_\odot$. The kinetic temperatures for protons ($T_{k,p}$) and the O^{5+} ions ($T_{k,O}$) are derived as a function of height with preferential heating of O^{5+} over protons recorded. By examining how $T_{k,p}$ varies with latitude at each height, an idea of the magnetic field morphology is found. At 1.75 $R_\odot$ the elemental abundances (O, S, Ar, and Fe), electron temperature, and electron density are derived from the UV spectral data. All three streamers were quiescent with typical abundance values; however, no depleted cores were found. The first ionization potential (FIP) effect was detected for all three streamers with a bias of ~4. This is consistent with slow solar wind in situ measurements, thereby supporting the hypothetical connection between the two. All three streamers had a higher than expected electron temperature. The electron densities above 1.75 $R_\odot$ are derived from the Large Angle Spectroscopic Coronagraph (LASCO) C2 polarized brightness data. Estimates for the O^{5+} outflow velocities are obtained using the O vi λ1032 over λ1037 intensity ratios and the estimated electron densities. All three streamers showed evidence of significant outflows at 4.0 and 5.0 $R_\odot$.

Subject headings: solar wind — Sun: abundances — Sun: corona

1. INTRODUCTION

The Ultraviolet Coronagraph Spectrometer (UVCS) (Kohl et al. 1995) aboard the *Solar and Heliospheric Observatory* (*SOHO*) has been conducting a streamer study that began in December of 2002. The goal is to analyze, as completely as possible, a variety of plasma properties for an individual streamer. The results are then cataloged with those from other streamers over the course of the solar cycle. This paper is the second in a series reporting the latest results from this study. The first paper (Uzzo et al. 2006, hereafter Paper I) examined the first of the three streamers reported here. It also provided a detailed overview of the techniques used to derive the streamer plasma properties. Therefore, the explanation of how the results were derived will be condensed, and interested parties are directed to Paper I for the details.

The reason for this second paper is threefold. Paper I examined a streamer observed in April of 2003, named Str030428 for this study, and was analyzed using the UVCS Data Analysis Software (DAS) version 3.4. In early 2006 DAS version 4.0 was released and the data for Str030428 were reanalyzed. The major advance of version 4.0 is an update in the radiometric calibrations, which had an impact on the numerical results for several plasma parameters, although not on the overall conclusions. For more information on UVCS calibrations the reader is directed to Pernechele et al. (1995) and Gardner et al. (1996). Data calibration uncertainties are discussed by Gardner et al. (2000). The second reason for this second paper is the inclusion of two additional streamers observed in 2003 May (Str030509) and September (Str030925). These two streamers had many of the same characteristics as Str030428 and serve to reinforce the conclusions from the first streamer. Whenever a reference is made to "the three streamers" it should be understood that it indicates Str030428, Str030509, and Str030925. The final reason for the second paper is the inclusion of how the proton kinetic temperature of the plasma varied with latitude and height. By examining this plasma parameter new details about the streamer magnetic morphology are potentially revealed.

As was the case in Paper I, a simple helmet streamer model is adopted for this study. The streamer model, illustrated in Figure 1, has a closed magnetic field "core" surrounded by open field lines. These flanking open field lines, referred to as the "legs," come together at the apex of the core at the location called the "cusp." From there the field lines extend nearly radially outward as the "stalk." It is the leg and stalk structures that have been identified as a potential source of the slow solar wind. Exploring any possible connection between streamers and the slow solar wind is one of the chief objectives of this streamer study. As explained in Paper I many authors have used a variety of techniques, such as abundances and outflow velocities, to investigate this hypothesis (e.g., Raymond et al. 1997; Habbal et al. 1997; Sheeley et al. 1997; Woo & Martin 1997; Wang et al. 1998; Strachan et al. 2002; Uzzo et al. 2003).

In § 2 the observations and the streamer morphologies are discussed. In § 3 the contributions to the total measured O vi doublet and H i Lyman series intensities originating from electron collisional excitation versus radiative excitation (resonant scattering of disk radiation) are covered. In § 4 the electron temperature (T_e) and the electron density results are reviewed. The photospheric normalized absolute elemental abundances at 1.75 $R_\odot$ are presented along with their implications for the presence of a depleted core and the first ionization potential (FIP) effect in § 5. Section 6 covers the perpendicular kinetic temperatures of the protons ($T_{k,p}$) and the O^{5+} ions ($T_{k,O}$). All of the above parameters are used to constrain the O^{5+} radial outflow velocity, which is described in § 7. The final section (§ 8) is a comparison of the results presented here, and those from previous publications are also given along with our conclusions. It should be noted that all results presented here are averaged between specific UVCS field of view (FOV) spatial boundaries and time averaged over the respective observation data sets.

2. OBSERVATIONS AND STREAMER MORPHOLOGY

To investigate the structures at the base of these streamers the images from the Mauna Loa Solar Observatory (Mk4) coronal

[1] Harvard-Smithsonian Center for Astrophysics, 60 Garden Street, Cambridge, MA 02138.
[2] Naval Research Laboratory, 4555 Overlook Avenue SW, Washington, DC 20375.

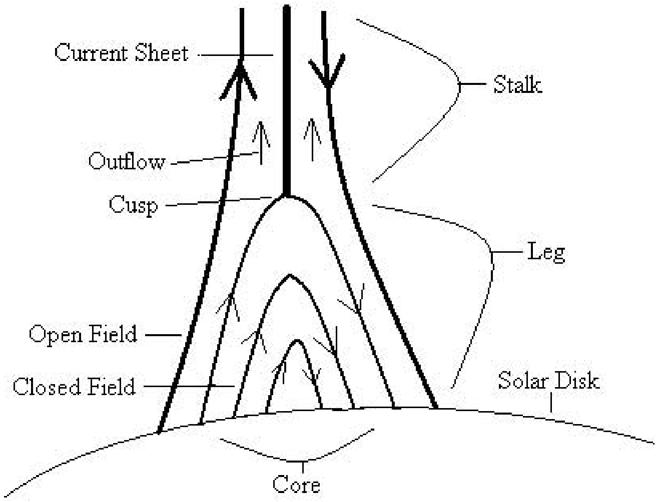

Fig. 1.—Simple streamer model diagram with labeled structures.

visible light and the Big Bear Solar Observatory Hα data are examined in addition to *SOHO* data. Electron densities above 2.2 $R_\odot$ were derived from the *SOHO* Large Angle Spectroscopic Coronagraph (LASCO) C2 polarized brightness (pB) synoptic observations. From these observations the electron scattered component, or K corona, is isolated, which then provides the electron density. Since the streamer morphology along the line of sight (LOS) is unknown azimuthal symmetry was assumed, and the electron densities reported here should be considered a lower bounds. To reduce the impact due to this azimuthal symmetry approximation the electron densities for the three streamers will be derived from data obtained near the time when the streamer reached the peak radial height. This should correspond to when the streamer base was centered at the limb. Further information concerning LASCO is provided in Brueckner et al. (1995). The remaining plasma parameters presented here were derived from the UVCS observations using spectroscopic diagnostic techniques.

The UVCS streamer study uses two types of observations, which are summarized in Table 1. The first type (I in Table 1) of observation is designed to optimize the intensity measurements of the weaker minor ions. The second type (P in Table 1) of observation uses an instrument configuration that is optimized for obtaining Lyα and O vi λ1032 spectral line profiles. The data for Figures 5–7 and Figures 12–14 are resampled to a spatial dimension resolution of 4.7′ to provide sufficient statistics. For the results of Tables 3–5 and Figure 11 the plasma parameters are derived using a resampling of the data over the streamer domain defined within the vertical dashed lines in Figures 5–7 for the three streamers, respectively. The coronal emission lines included in this study are the following: the O vi doublet ($\lambda\lambda$1032 and 1037), H i Lyα (λ1215), H i Lyβ (λ1025), H i Lyγ (λ972), [Fe x] (λ1028), [Fe xii] (λ1242), [Fe xiii] (λ510), Ar xii (λ1018), and S x (λ1196). The spectral binning was set to 2 pixels bin^{-1} except for the O vi doublet panel of the profile studies, which had a 1 pixel bin^{-1} setting. Most of the lines listed above come from the primary path of the O vi detector, which has a 0.0993 Å pixel^{-1} resolution. The Lyα, [Fe xii], and S x lines come from the O vi detector redundant path, which has a 0.091 Å pixel^{-1} resolution. The Lyα line is obtained from the profile study, while the O vi doublet is obtained in both the intensity and profile studies. The remaining lines listed above are obtained through the combination of the three grating positions listed in Table 1 at 1.75 $R_\odot$. It should be noted that the Si xii (λ499) line reported in Paper I has been dropped from this study due to significant uncertainty in this second-order line intensity calibration and in the atomic rates for this Li-like ion (Laming & Feldman 1999). From the data the T_e, electron densities, and photospheric normalized absolute elemental abundances at 1.75 $R_\odot$ were derived. The profile observations include H i Lyα (λ1215) and the O vi doublet ($\lambda\lambda$1032 and 1037) at 1.75, 2.5, 3.0, 4.0, and 5.0 $R_\odot$. That data allow the derivation of the O^{5+} outflow velocity as well as $T_{k,\mathrm{O}}$ for the O^{5+} ions and $T_{k,p}$ for the protons.

TABLE 1

Observation Parameters

Height ($R_\odot$)	Type[a]	Grating[b] (EU)	Slit (μm)	Duration (hr)
1.75	I	236900	100	3.73
1.75	I	225000	100	1.87
1.75	I	103000	100	1.87
1.75	P	175604	50	1.07
2.50	P	175604	50	2.93
3.00	P	175604	50	5.33
4.00	P	175604	150	5.33
5.00	P	175604	150	9.07

[a] I = intensity study, P = profile study; see text.
[b] O vi detector grating position in engineering units.

Composite images showing the three streamers and their surrounding regions on and off the disk are provided as Figures 2–4. The three figures are given in the chronological order Str030428, Str030509, and Str030925, respectively. Each figure has four panels. For the first panel (*a*) working from the outside inward are images from LASCO C2, Mk4, and the Extreme-ultraviolet Imaging Telescope (EIT; Delaboudinière et al. 1995) at 195 Å. The dark lines indicate the approximate locations of the UVCS FOVs relative to each streamer. The second panel (*b*) shows the Mk4 and EIT images of the first panel in greater detail. The component images of panels (*a*) and (*b*) are not to scale. Their purpose is to examine the local environment and help identify which structures are located under the streamers. Panel (*c*) is an Hα image, and panel (*d*) is a magnetogram image from the Michelson Doppler Imager (MDI) on *SOHO* (Scherrer et al. 1995).[3] The dates and times for the images used to construct Figures 2–4 are listed in Table 2. Also provided in Table 2 are the start dates and times for the UVCS observations that are used in the streamer designations.

The first two streamers were located at the northeast limb, both centered at $\sim$55° counterclockwise from solar north. The images that comprise Figures 2 and 3 were made after the start of the corresponding UVCS observations. For the two white-light images, this provides the streamer's morphology at a time closer to the midpoint of the UVCS observations. In the case of the EIT, Hα, and MDI images it allowed solar rotation to bring the structures located at the base of the streamer into view on the disk. For Str030925, which was observed at the northwest limb (centered at position angle $\sim$320°), the EIT, Hα, and MDI images selected were taken before the UVCS observation. To minimize the effects of solar rotation (Uzzo et al. 2003) on the results, the UVCS observations were completed within a 2 day period. The total duration for the three UVCS observations are provided in the notes to Table 2.

The three streamers presented here were chosen from the catalog due to their well-defined helmet structure and their stability. These are two qualities that are difficult to obtain near solar maximum. It should be noted that unlike Str030428, the streamers

[3] These last two images were obtained from the Active Region Monitor at http://www.solarmonitor.org.

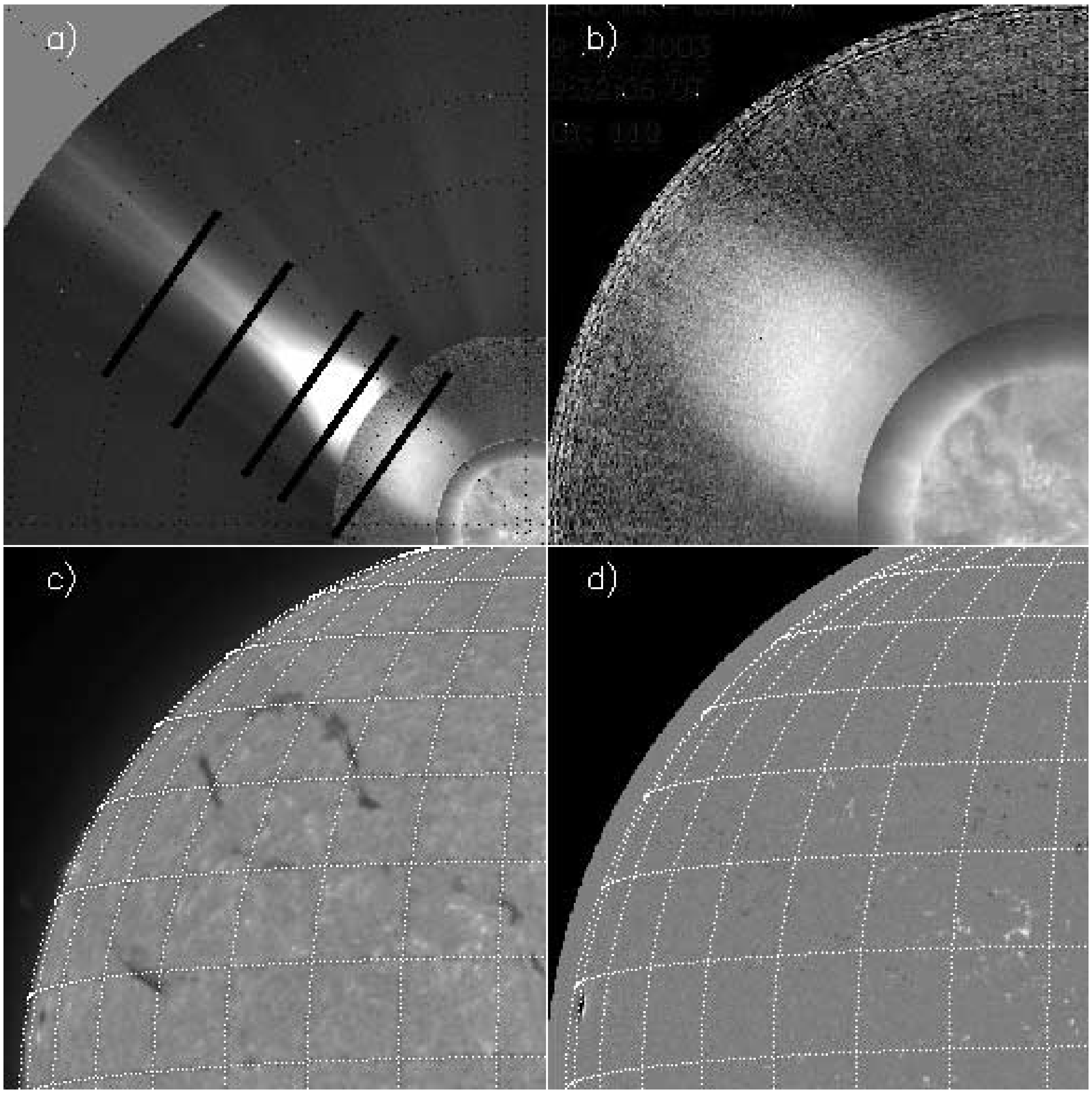

FIG. 2.— Solar conditions at the location of the streamer observation designated Str030428. The four component images are (*a*) C2, Mk4, and EIT; (*b*) Mk4 and EIT; (*c*) Hα; and (*d*) MDI. The five UVCS observation heights (1.75, 2.5, 3.0, 4.0, and 5.0 $R_\odot$) are represented by the black bars in (*a*). The component images of (*a*) and (*b*) are not to scale. See text for details.

Str030509 and Str030925 did not form above a clearly defined extended prominence. In addition, minor contributions from ARs 10356 and 10460, which were located south of Str030509 and Str030925, respectively, cannot be entirely ruled out from the UVCS results. We use the three composite images in Figures 2–4 to demonstrate that all three streamers were quiescent and not active region streamers. The arguments for Str030428 (Fig. 2) are provided in Paper I. For Str030509 (Fig. 3) the lowest latitude grid line in panels (*c*) and (*d*) represents the equator. The only active region near the streamer was AR 10356, which was $\sim 20^\circ$ latitude from the streamer and $\sim 30^\circ$ in longitude from the limb when the UVCS observation started. Since Str030509 was located near latitude 55° and interpreting the location in panels (*a*) and (*b*) of Figure 3 relative to this active region, it can be concluded that this streamer was most likely not associated with the active region. It was therefore classified as a quiescent streamer. For Str030925 (Fig. 4) AR 10460 was located $\sim 55^\circ$ from the limb in longitude and $\sim 40^\circ$ in latitude from the streamer at the start of the observation. Based on the separation between AR 10460 and the base of Str030925, as well as examining the structures shown in panels (*a*) and (*b*) of Figure 4, it can be concluded that this streamer was also a quiescent. For all three cases there were no active regions located directly in front of or behind the base of the streamers.

The O VI $\lambda 1032$ (*solid lines*) and the Lyα (*dashed lines*) intensity distributions across the latitudinal dimension of Str030428, Str030509, and Str030925 are provided in Figures 5–7, respectively. These intensity distributions are each normalized to a peak intensity of 5. The vertical dashed lines represent streamer boundaries. The square and diamond data points indicate values for the calculated oxygen abundances, which is discussed in § 5. The presence of an abundance depletion in the core structure of a streamer can be investigated by comparing the O VI and Lyman series intensity profiles. As shown in Figure 4 from Uzzo et al. (2004), when the O VI intensity has a double peak and the location of the central minimum corresponding to the single peak maximum of the Lyman series profile, a depleted core may exist. The circles and crosses represent the $T_{k,\mathrm{O}}$ and $T_{k,p}$, respectively.

3. COLLISIONAL AND RADIATIVE INTENSITY COMPONENTS

In order to derive several of the streamer plasma parameters at 1.75 $R_\odot$ any radiative component must be separated from the total line intensity. The spectral lines of the H I Lyman series and

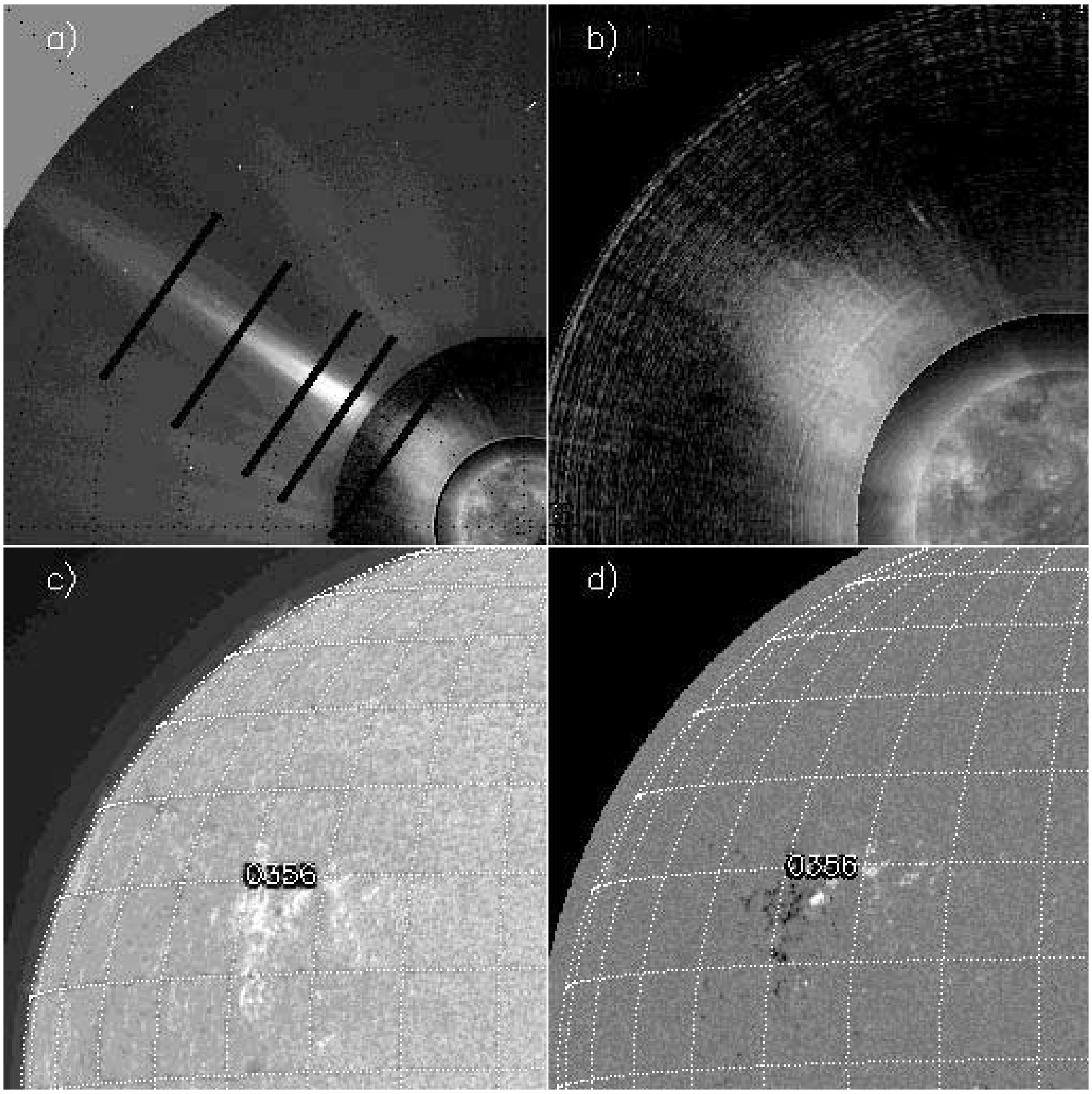

FIG. 3.—Same as Fig. 2, but for Str030509.

the O VI doublet each have radiative and collisional contributions. To separate the individual radiative and collisional components the same procedures outlined in Paper I are followed. As shown in Paper I, the radiative and collisional contributions to each line of the O VI doublet can be determined from the known ratios of the separate O VI intensity components. They are 4 : 1 for the radiative components and 2 : 1 for the collisional components. These relations are strictly true only if there is no radial outflow velocity. Based on the radial outflow velocity results for these three streamers (see § 7) these expressions can be used in the analysis at 1.75 $R_\odot$.

Separating the collisional and radiative contributions from the observed Lyβ intensity can be made using the Lyα to Lyβ or Lyβ to Lyγ intensity ratio. However, complications arise because the disk intensities (the inputs for the resonant scattering) in general are not emitted from a uniform Sun. The Lyman series disk intensities vary depending on the percentage that originate from active regions versus quiet Sun. On the disk the coronal hole and quiet-Sun intensities are approximately equal when compared to the active region intensity. From the disk intensities published by Vernazza & Reeves (1978), the Lyβ to Lyγ intensity ratio is independent of the source structure to within 2.6%. This is not true for the intensity ratio of Lyα over Lyβ. Although the Lyγ line is much weaker than Lyα, the radiative and collisional derived oxygen abundances agree significantly better when Lyγ is used. Further discussion of this topic is located in § 5. Instead of using the disk intensity values provided by Vernazza & Reeves (1978), we will employ the values listed in Raymond et al. (1997) from UVCS on disk observations. Those values are 4.13 and 0.867 in units of 10^{13} photons cm^{-2} s^{-1} sr^{-1} for Lyβ and Lyγ, respectively. This removes the issue of different instrument calibrations from the equation. The result is a radiative component of Lyβ/Lyγ of 14.36, while the collisional component is 3.02 (see Paper I).

Using the Lyβ/Lyγ intensity ratio the collisional and radiative components are separated independent of their disk source, and then the abundances are derived. However, calculating the electron density below the C2 occulting disk requires an additional step. The electron density at 1.75 $R_\odot$ is derived using UVCS data and requires the O VI λ1032 disk intensity. To derive this value the amount of solar disk radiation coming from active regions versus quiet Sun at 1.75 $R_\odot$ must be determined. This can be accomplished by using equation (1), where η is a free parameter between

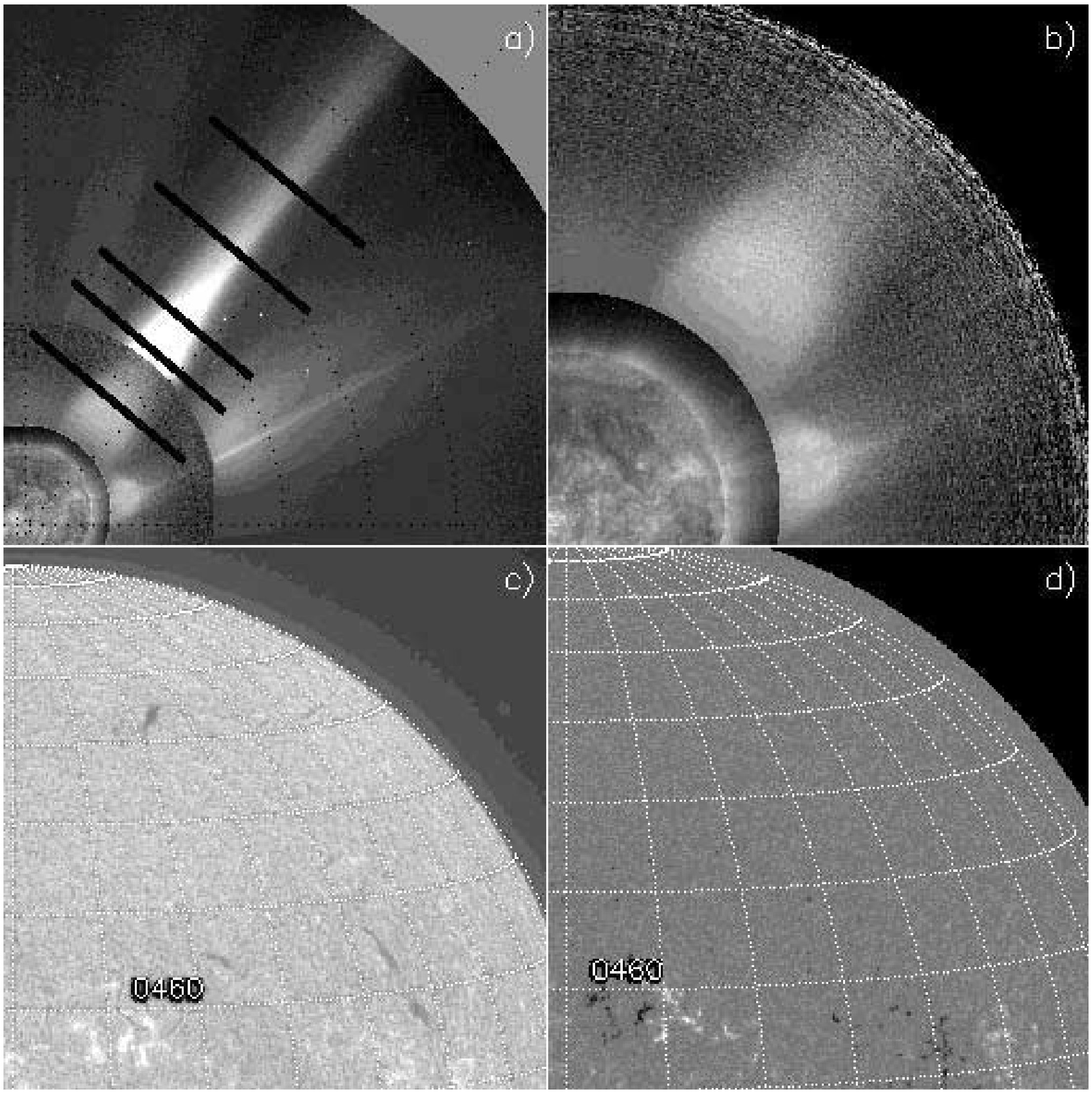

FIG. 4.—Same as Fig. 2, but for Str030925.

zero and 1 that represents the fraction of the integrated disk intensity due to active regions:

$$I_i(\text{disk}) = \eta I_i(\text{active}) + (1 - \eta) I_i(\text{quiet}). \quad (1)$$

Using the approach in Paper I, the radiative and collisional components of Lyβ are separated using Lyγ. Next the components for Lyβ are rederived using Lyα instead of Lyγ and equation (1) substituted in place of the constant disk intensities with η equal to zero. The parameter η is then increased until the results for Lyβ radiative and collisional using the Lyα intensity agree with those from Lyγ. Using this optimal η, plus the active region and quiet-Sun intensities for O VI λ1032 the effective O VI disk intensity can be derived by equation (1). The η results for

TABLE 2
STREAMER OBSERVATIONS

	Str030428		Str030509		Str030925	
Observation	Date	Time (UT)	Date	Time (UT)	Date	Time (UT)
UVCS	2003 Apr 28	16:56[a]	2003 May 09	19:58[b]	2003 Sep 25	18:18[b]
LASCO C2	2003 Apr 29	21:26	2003 May 10	21:54	2003 Sep 25	20:30
Mk4	2003 Apr 29	19:32	2003 May 10	19:01	2003 Sep 25	17:49
EIT 195	2003 Apr 29	23:12	2003 May 10	22:24	2003 Sep 23	11:23
Hα	2003 Apr 30	22:00	2003 May 11	21:00	2003 Sep 22	17:00
MDI	2003 Apr 30	21:28	2003 May 11	21:28	2003 Sep 22	00:00

[a] Observation completed after 39.5 hr.
[b] Observation completed after 43.5 hr.

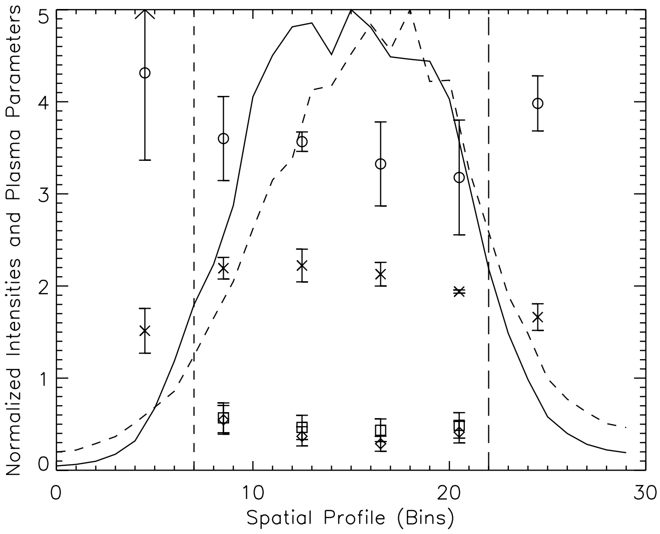

FIG. 5.— Str030428 spatial profiles along UVCS FOV of the O VI λ1032 intensity (*solid line*) and the intensity of Lyα λ1215 (*dashed line*) at 1.75 $R_\odot$ (1 bin = 70″). The spectral widths of these two lines produce the oxygen (*circles*) and proton kinetic temperatures (*crosses*), respectively. The oxygen abundances are derived from the collisional (*squares*) and radiative (*diamonds*) intensity data. Note: the intensity curves are normalized to a peak of 5 for both the O VI (O VI/2.907×10^9) and Lyα (Lyα/7.679×10^{10}) profiles.

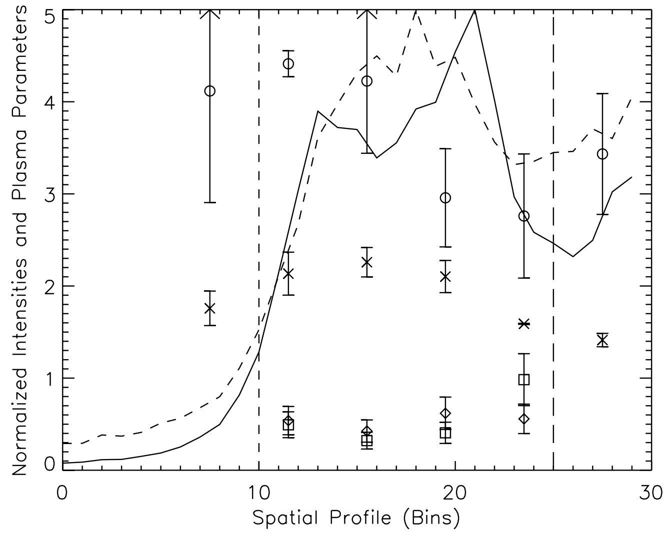

FIG. 7.— Same as Fig. 5 for Str030925, except the normalized intensity spatial profiles are O VI/2.758×10^9 and Lyα/5.433×10^{10}.

Str030428, Str030509, and Str030925 are 0.62, 0.20, and 0.52, respectively.

4. ELECTRON TEMPERATURE AND ELECTRON DENSITY

One technique to derive the averaged T_e along the LOS uses the intensities from several ions of the same element, such as iron, and the collisional intensity of the Lyβ line. For the three streamers the iron lines employed are [Fe X], [Fe XII], and [Fe XIII]. The term $R_{\rm obs}$ is defined as the ratio of the iron line intensity to the Lyβ collisional intensity. The $R_{\rm th}$ term is the theoretical ratio of each iron ion emissivity over the Lyβ emissivity. The emissivity values come from the CHIANTI version 5 database (Dere et al. 1997; Landi & Phillips 2005). The ionization balances are from Mazzotta et al. (1998), and Grevesse & Sauval (1998) provide the photospheric abundances except for the oxygen abundances, which come from Asplund et al. (2004). The $R_{\rm th}$ are functions of T_e, so the ratio $R = R_{\rm th}/R_{\rm obs}$ are plotted as $\log_{10}(R)$ versus $\log_{10}(T_e)$. This is done for each iron ion by the solid curves, as presented in Figure 8 (Str030428), Figure 9 (Str030509), and Figure 10 (Str030925).

The value for T_e is derived by averaging the x-axis values where each pair of solid line curves intercept. The average of the intercepts is denoted by the square in Figures 8–10 at 1.82 ± 0.24, 1.65 ± 0.20, and 1.75 ± 0.23 MK for the three streamers, respectively. These results are also listed in Table 3. The T_e could only be derived at 1.75 $R_\odot$ due to the absence of any Fe line emissions at the upper heights. For the case of an ideal isothermal plasma, all three curves would intercept at the same location in each of the three figures. Since this is not the case for any of the streamers, there is the possibility that there are discrete regions of different T_e along the LOS. However, in the absence of additional data, the plasma was taken as isothermal. We should mention

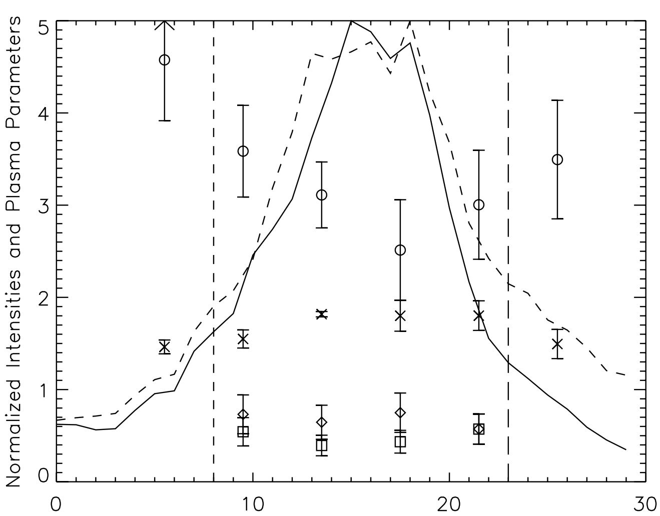

FIG. 6.— Same as Fig. 5 for Str030509, except the normalized intensity spatial profiles are O VI/4.236×10^9 and Lyα/7.383×10^{10}.

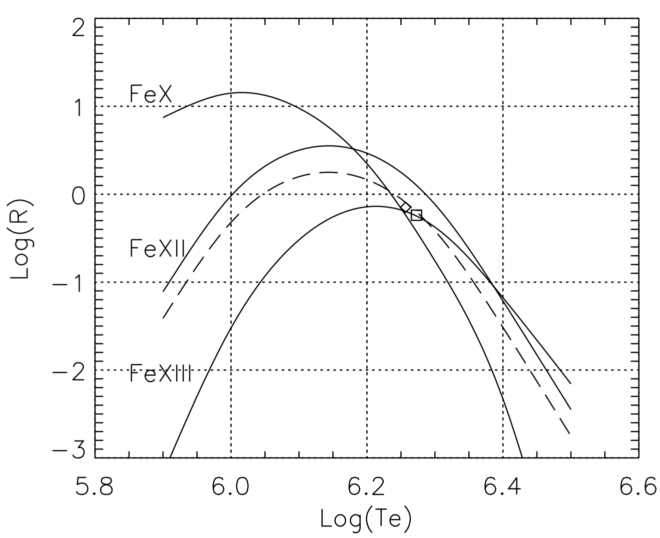

FIG. 8.— Plot of $\log_{10}(R)$ (CHIANTI ver. 5) vs. $\log_{10}(T_e)$ for the three ions [Fe X], [Fe XII], and [Fe XIII] (*solid lines*) used to derive an average T_e for the streamer plasma of approximately 1.82 ± 0.24 MK (*square*) at 1.75 $R_\odot$. The dashed curve represents the [Fe XII] emissivity modified by a factor of 0.5, resulting in an average $T_e = 1.75\pm0.21$ MK (*diamond*). See text for the definition of R.

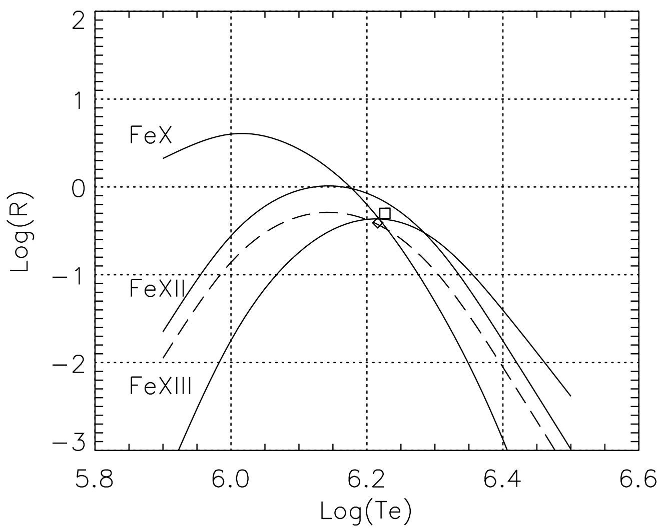

Fig. 9.—Same as Fig. 5, except for Str030509 with T_e equal to 1.65 ± 0.20 MK (*square*) and 1.61 ± 0.19 MK (*diamond*) for the modified Fe emissivity.

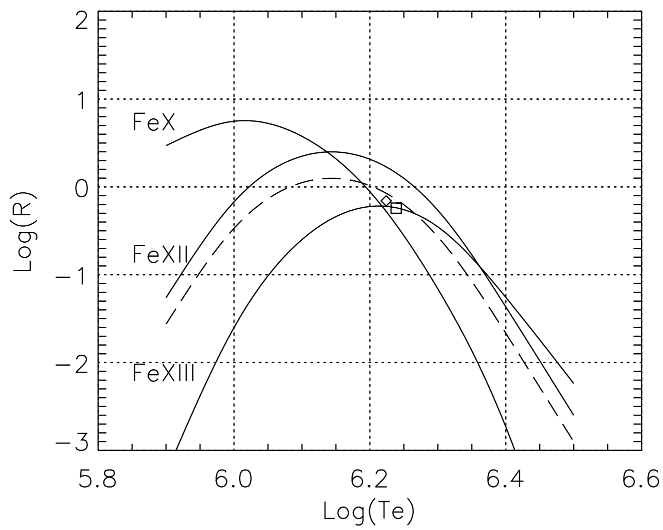

Fig. 10.—Same as Fig. 5, except for Str030925 with T_e equal to 1.75 ± 0.23 MK (*square*) and 1.70 ± 0.21 MK (*diamond*) for the modified Fe emissivity.

that two additional iron lines were detected in the data for all three streamers. These lines, Fe xv λ481 and [Fe xviii] λ974, did not have a high count rate and therefore had extremely large uncertainties in their intensities. Although the presence of these two high T_e formation lines suggests the presence of a multithermal plasma along the LOS (Parenti et al. 2000), their lack of sufficient counts prevents the application of a multithermal analysis, as done by Ko et al. (2002). For this reason neither line was applied to the isothermal analysis mentioned above.

Note that there is no consensus on the best values to use for the [Fe xii] emissivities (Raymond et al. 1997; Ko et al. 2002; Paper I). According to Binello et al. (2001) a large discrepancy exists among the theoretical excitation rates for this ion as well as discrepancies between models and observed spectra. As an experiment the [Fe xii] emissivity was modified by a factor of 0.5, and the results are shown as the dashed curve in each $\log_{10}(R)$ versus $\log_{10}(T_e)$ plot. Now the intercepts of [Fe x], [Fe xiii], and the modified [Fe xii] have a near common intercept for each of the three streamers, represented by the diamond in each figure. The impact of using the modified [Fe xii] emissivity was a less than 4% decrease in the resulting T_e for all three streamers (1.75, 1.61, and 1.70 MK, respectively). The convergence of the intercepts provides additional support to the assumption of an isothermal plasma. However, it is not clear if these results alone are sufficient justification for accepting the modification to the [Fe xii] emissivity. Therefore, the results for the three streamers given in Tables 3–5 are all derived using the original CHIANTI version 5 emissivities.

The streamer electron densities were determined using two methods: one using the usual white-light coronograph observations and the other using the O vi doublet intensity ratios from UVCS observations (Parenti et al. 2000). For heights above 2.25 $R_\odot$ the LASCO C2 pB data can be used to estimate the electron density. The results for 2.5, 3.0, 4.0, and 5.0 $R_\odot$ are provided in Table 5 for the three streamers examined here. The sources of uncertainty for these electron densities are briefly outlined in Strachan et al. (2002) and were found to be approximately 50%. To derive the value of the electron density for heights below the C2 occulting disk, the observed O vi doublet line properties, the derived T_e, and the O vi λ1032 disk intensity can be applied to equation (3) of Paper I. The parameter I_{1032}(disk) is derived using equation (1) and the estimates for η, as described in § 3. As previously stated, the density estimate determined with this method is valid for negligible radial outflow. The 1.75 $R_\odot$ electron density results for the three streamers are provided in Table 3 as well as Table 5.

5. ELEMENTAL ABUNDANCES AND THE FIP EFFECT

In this section we report on the absolute abundances of oxygen, sulfur, argon, and iron normalized by their photospheric values. The absolute abundance refers to the elemental abundance divided by the hydrogen abundance. As described in Paper I, the abundance for a given element can be calculated by using either the radiative or collisional intensities. Only the O vi doublet has a nonnegligible radiative intensity component, and so will be the only minor ion with its abundance calculated both ways. Ideally these two results should be equal. The oxygen abundance derived from the radiative intensity was calculated using equation (4) of Paper I, while the abundances for oxygen, sulfur, argon, and iron used the collisional line intensities and equation (6) of Paper I. The line intensities are averaged over the sampled spatial region, denoted by the vertical dashed lines in Figures 5–7. See Paper I for a more complete description. It should be noted that none of the emissivities for the observed spectral lines reported here vary significantly as a function of the electron density at streamer values. Therefore, a fixed electron density of 1×10^7 cm^{-3} was used to generate the theoretical emissivities with CHIANTI. The electron densities derived at 1.75 $R_\odot$ for the three streamers in the previous section agree with this fixed value.

Table 3 shows the calculated oxygen abundance, normalized to its photospheric value, for all three streamers studied. For Str030428, Str030509, and Str030925 the abundances derived from the collisional intensities are 0.47 ± 0.13, 0.45 ± 0.13, and 0.43 ± 0.12, respectively, while the abundances calculated from the radiative intensities are 0.37 ± 0.10, 0.67 ± 0.19, and 0.53 ± 0.15, respectively. The discrepancy between the oxygen abundances using the two methods are 21%, 49%, and 23%, respectively, using the collisional value as the accepted result. The abundances for oxygen, sulfur, argon, and iron using the collisional intensities are provided in Table 4. The iron results for each streamer were derived by averaging the abundances calculated from [Fe x], [Fe xii], and [Fe xiii]. As a reminder, all tabulated results were calculated using unmodified emissivities provided by the CHIANTI version 5 database.

In addition to calculating the absolute abundances averaged across the streamer width for all of the elements, it is also interesting

TABLE 3

Oxygen Abundance, Electron Temperature, and Electron Density

Source	Height ($R_\odot$)	Type[a]	$[O/H]/[O/H]_{ph}$[b] Collisional	Radiative	T_e (MK)	N_e (10^6 cm^{-3})
Str030428	1.75	QS	0.47 ± 0.13	0.37 ± 0.10	1.82 ± 0.24	32.21 ± 9.40
Str030509	1.75	QS	0.45 ± 0.13	0.67 ± 0.19	1.65 ± 0.20	10.76 ± 3.15
Str030925	1.75	QS	0.43 ± 0.12	0.53 ± 0.15	1.75 ± 0.23	18.27 ± 5.38
Uzzo et al. (2004)	1.75	AL	0.92[c]	...	1.55	...
Uzzo et al. (2004)	1.75	AC	0.28	...	1.66	...
Bemporad et al. (2003)	1.60	AL	0.68[d]	...	1.20	27.00
Bemporad et al. (2003)	1.60	AC	0.54[d]	...	1.41	53.00
Bemporad et al. (2003)	1.90	AL	1.02[d]	...	1.17	11.60
Bemporad et al. (2003)	1.90	AC	0.58[d]	...	1.32	18.90
Raymond et al. (2003)[e]	1.64	AL	1.06	...	1.34	4.80
Raymond et al. (2003)[e]	1.64	AC	0.60	...	1.37	5.30
Raymond et al. (2003)[f]	1.64	AL	0.81	...	1.40	5.40
Raymond et al. (2003)[f]	1.64	AC	0.78	...	1.42	3.90
Raymond et al. (2003)[g]	1.64	AL[h]	0.70	...	1.41	4.50
Raymond et al. (2003)[g]	1.64	AC	0.31	...	1.60	4.60
Marocchi et al. (2001)[i]	1.70	QL	0.37	0.63	1.58[j]	...
Marocchi et al. (2001)[i]	1.70	QC	0.06	0.22	1.58[j]	...
Parenti et al. (2000)[k]	1.60	AR	0.12	0.34	1.23	3.30
Parenti et al. (2000)[l]	1.60	AR	0.26	0.49	1.28	7.47
Li et al. (1998)	1.50	QC	0.14	...	1.58	13.00
Raymond et al. (1997)	1.70	AR	0.44	1.07	1.58[j]	...
Raymond et al. (1997)	1.50	QL	0.43	0.63	1.58[j]	...
Raymond et al. (1997)	1.50	QC	0.11	0.15	1.58[j]	...

[a] Streamer classification: AR = active region; AL = active region leg; AC = active region core; QS = quiescent; QL = quiescent leg; QC = quiescent core.
[b] Normalized using photospheric abundance from Asplund et al. (2004).
[c] Average of two leg results.
[d] Average of collisional and radiative results.
[e] Streamer observed 2002 April 21.
[f] Streamer observed 2002 July 23.
[g] Streamer observed 2002 August 24.
[h] First leg results.
[i] Streamer observed 1996 April 11.
[j] Assumed value.
[k] Equatorial streamer observed 1998 March 8.
[l] Midlatitude streamer observed 1998 March 8.

to look for abundance variations as a function of latitude or distance across the streamer. This was done in earlier studies (e.g., Raymond et al. 1997) to identify abundance depletion in the streamer core. For the present study only the oxygen lines were bright enough to make discrete intensity measurements for multiple latitude bins. The photospheric normalized absolute abundances for oxygen are indicated by the square (collisional) and diamond (radiative) data points in Figures 5, 6, and 7 for the three streamers. Each data point in these three figures represents a resampling of the data into bins of $\sim 4.7'$ to increase the statistical accuracy. With one exception covered shortly, the abundances at each bin derived from the radiative and collisional intensities are in reasonable agreement. To detect the presence of any possible depleted cores an average of the collisional and radiative abundances are considered at each bin across each individual streamer, respectively. Typically a streamer has an abundance-depleted core if the abundance ratio of leg to core structures is typically 10 : 1 for well-defined cores (Raymond et al. 1997; Uzzo et al. 2003). The maximum leg to core ratios for the averaged oxygen abundances are 1.6, 1.3, and 2.1 for Str030428, Str030509, and Str030925, respectively. It can therefore be concluded that all three streamers in the present study lack the strong abundance depletion seen in other quiescent streamers.

The one case in which the radiative and collisional abundances do not agree very well is bin 23 of Str030925 (Fig. 7). At bin 23 the collisional abundance has a much higher than expected value (~ 1.0). This collisional abundance anomaly could be due to the presence of a second structure located south of Str030925, as shown in Figure 4. The presence of a second structure along the LOS is supported by the significant increase in both line intensities shown in Figure 7 along the southern edge of the streamer. If the T_e of the second structure is lower than the derived value for Str030925, the result at bin 23 would be a weighted average T_e of the two. If the T_e used to derive the oxygen collisional abundance (1.75 MK) was sufficiently higher than this weighted average, the outcome would be an inaccurately high abundance result. The T_e has a maximum possible value equal to the $T_{k,p}$. As shown in Figure 7 the $T_{k,p}$ at bin 23 is 1.59 MK, which is significantly lower compared to the average $T_{k,p}$ of the remaining streamer, at 2.16 MK. Therefore, it is reasonable that the weighted average T_e at bin 23 is significantly lower than the 1.75 MK used in the calculation.

Next we turn to the first ionization potential (FIP) effect, which is a phenomenon where the photospheric normalized abundances of low-FIP elements (i.e., FIP $<$ 10 eV) are more abundant compared to high-FIP elements (i.e., FIP $>$ 10 eV; Geiss 1982). The 10 eV boundary may be related to the energy available

TABLE 4

PHOTOSPHERIC NORMALIZED ABSOLUTE ELEMENTAL ABUNDANCES AT 1.75 $R_\odot$

Source	Height ($R_\odot$)	Type[a]	Collisional O	Collisional S	Collisional Ar	Collisional Fe
Str030428	1.75	QS	0.47 ± 0.13	0.20 ± 0.06	0.60 ± 0.17	1.77 ± 0.42[b]
Str030509	1.75	QS	0.45 ± 0.13	0.23 ± 0.07	0.46 ± 0.13	2.13 ± 0.50[b]
Str030925	1.75	QS	0.43 ± 0.12	0.16 ± 0.05	0.76 ± 0.22	1.84 ± 0.44[b]
Uzzo et al. (2004)	1.75	AL[c]	0.92	0.88	0.85	4.78[d]
Uzzo et al. (2004)	1.75	AC	0.28	0.23	0.27	1.28[d]
Bemporad et al. (2003)	1.60	AR	0.61[e]	0.12	...	1.15
Bemporad et al. (2003)	1.90	AR	0.80[e]	0.15	...	1.20
Ko et al. (2002)	1.60	AR	0.43	0.22	0.46	1.59
Li et al. (1998)	1.50	QC	0.14	0.06	0.07	0.48
Raymond et al. (1997)	1.70	AR	0.69	0.19	0.63	0.79
Raymond et al. (1997)	1.50	QL	0.55	0.19	0.50	1.00
Raymond et al. (1997)	1.50	QC	0.14	0.07	...	0.32
FIP state	...	...	High	High	High	Low
Photospheric abundances[f]	...	...	8.66	7.33	6.40	7.50

NOTE.—Normalized using photospheric abundances provided in last row.

[a] Streamer classification: AR = active region; AL = active region leg; AC = active region core; QS = quiescent; QL = quiescent leg; QC = quiescent core.

[b] Abundance derived from averaged Fe abundances.

[c] Averaged results of two leg structures.

[d] Abundance derived from Fe XII intensity.

[e] Average of collisional and radiative results.

[f] Absolute photospheric abundances of Grevesse & Sauval (1998) and Asplund et al. (2004) for oxygen in dex format used to normalize.

for ionization by Lyα photons (Raymond 1999). As expected (see Table 4) the high-FIP elements oxygen, sulfur, and argon are depleted relative to their photospheric values, while iron, a low-FIP element, is enhanced for all three streamers. The FIP effect is often examined in terms of the FIP bias, which is the ratio of a low-FIP element over a high-FIP element, usually oxygen. As discussed in Paper I and references therein, this leads to an ambiguity about whether the FIP bias is due to an enhancement of the low-FIP element or a depletion of the high-FIP element. The ambiguity can be resolved by examining the absolute abundances. For the present study it is found that both low-FIP enhancement and high-FIP depletion are present. In many of the earlier coronal abundance studies a hydrogen abundance was not available, so the FIP bias was employed. A FIP bias of approximately 4 is typically found in both coronal streamers and the slow solar wind (Raymond et al. 1997, 2001; Feldman et al. 1998; Raymond 1999; Parenti et al. 2000; Uzzo et al. 2003). In the present study, a FIP bias (iron over oxygen) of 3.77 for Str030428, 4.73 for Str030509, and 4.28 for Str030925 are calculated. These results are consistent with models of streamers as contributors to the slow solar wind.

6. PERPENDICULAR KINETIC TEMPERATURES

UVCS can measure spectrally resolved line profiles, which permits the "kinetic temperatures" of coronal ions to be determined. As shown in Paper I (eq. [7]) the $1/e$ half-width of a Gaussian fit to the coronal line profile can be converted to a LOS averaged kinetic temperature (T_k). Care must be taken to remove any instrument and background effects before making the profile fit (Kohl et al. 1997; Zangrilli et al. 1999). In practice, T_k is the sum of thermal ($T_{\mathrm{th},i}$) and nonthermal (ξ_i) contributions. From $T_{\mathrm{th},i}$ the microscopic velocity distribution is found, while the term ξ_i contains the bulk outflow velocity of the plasma along the LOS and may contain other nonthermal contributions such as those due to transverse wave motions.

Temperatures determined from the H I Lyman series line widths can be used as proxies for the proton temperatures, since streamer densities are large enough so that charge exchange will make the protons and neutral hydrogen have the same T_k (Vásquez et al. 2003). The $T_{k,p}$ and $T_{k,\mathrm{O}}$ are determined at the five heights 1.75, 2.5, 3.0, 4.0, and 5.0 $R_\odot$ in all three streamers. These values are reported in Table 5. If most of the streamer emission comes from near the plane of the sky, the LOS is essentially perpendicular to the streamer axis (and to the magnetic field); thus, the temperatures characterize the perpendicular motions of the ions. The electrons and protons at 1.75 $R_\odot$ can be assumed to be at thermal equilibrium due to the high density and low outflow velocity found within streamers at low heights (Li et al. 1998; Vásquez et al. 2003). From $T_{\mathrm{th},p} \approx T_e$ the resulting nonthermal components of Str030428, Str030509, and Str030925 are 0.31, 0.12, and 0.28 MK or converted to velocity 72, 44, and 68 km s^{-1}, respectively.

In Figures 5–7 the $T_{k,\mathrm{O}}$ (*circles*) and $T_{k,p}$ (*crosses*) are plotted across the streamer at 1.75 $R_\odot$. Due to the high intensity of the H I Lyα spectral line the $T_{k,p}$ can also be plotted across the streamer at the upper four heights for each streamer. The Lyα intensities and kinetic temperatures at the four highest heights in each streamer are plotted separately in the quad plots shown in Figures 12–14. The H I Lyα intensity across the slit for all 12 plots are normalized to a peak value of 5 for consistency with Figures 5–7. This allows the streamer and the surrounding environment to be analyzed as a function of the T_k, thus providing deeper insight into the morphology of the system.

7. OUTFLOW VELOCITIES

By using the Doppler dimming of the O VI doublet lines at 1032 and 1037 Å the radial outflow velocity of O^{5+} ions can be calculated (Withbroe et al. 1982; Noci et al. 1987; Strachan et al. 2000). As explained in Paper I and references therein, Doppler dimming affects only the radiative component of the coronal intensities. There are two approaches to modeling the system and thus deriving the outflow velocity. The first is to model each of the O VI lines separately. The second method is to model the intensity ratio of $\lambda 1032/\lambda 1037$, which is more convenient because it reduces

TABLE 5
Physical Parameters versus Height

Parameter	1.75 $R_\odot$	2.5 $R_\odot$	3.0 $R_\odot$	4.0 $R_\odot$	5.0 $R_\odot$
			Str030428		
T_k O vi (MK)	3.43 ± 0.45	4.08 ± 1.08	3.75 ± 0.77	6.64 ± 2.01	5.24 ± 3.86
T_k H i (MK)	2.13 ± 0.01	2.32 ± 0.19	1.96 ± 0.20	1.53 ± 0.14	1.32 ± 0.15
V_{out} (km s^{-1})	...	...	...	<20–63	102–127
N_e (10^6 cm^{-3})	32.21 ± 9.40	2.18 ± 1.09	0.87 ± 0.44	0.23 ± 0.12	0.09 ± 0.05
			Str030509		
T_k O vi (MK)	2.95 ± 0.48	3.16 ± 1.10	3.78 ± 1.00	7.83 ± 0.13	3.90 ± 2.73
T_k H i (MK)	1.77 ± 0.13	1.72 ± 0.19	1.49 ± 0.16	1.24 ± 0.11	0.95 ± 0.09
V_{out} (km s^{-1})	...	...	...	<20–73	106–137
N_e (10^6 cm^{-3})	10.76 ± 3.15	1.35 ± 0.68	0.63 ± 0.32	0.20 ± 0.10	0.05 ± 0.03
			Str030925		
T_k O vi (MK)	3.42 ± 0.62	3.88 ± 1.34	4.35 ± 1.28	6.83 ± 3.40	7.47 ± 2.12
T_k H i (MK)	2.03 ± 0.15	1.89 ± 0.29	1.61 ± 0.30	1.32 ± 0.19	1.36 ± 0.17
V_{out} (km s^{-1})	...	...	...	29–82	112–176
N_e (10^6 cm^{-3})	18.27 ± 5.38	1.06 ± 0.53	0.51 ± 0.26	0.13 ± 0.07	0.04 ± 0.02
			Strachan et al. (2002)		
T_k O vi (MK)	2.02 ± 0.02	9.10 ± 4.56	14.28 ± 3.57	15.79 ± 4.57	23.56 ± 6.65
T_k H i (MK)	1.96 ± 0.07	1.92 ± 0.06	1.58 ± 0.05	1.34 ± 0.08	1.24 ± 0.07
V_{out} (km s^{-1})	...	<20	<20	52	89
N_e (10^6 cm^{-3})	...	1.50 ± 0.75	0.73 ± 0.37	0.20 ± 0.10	0.11 ± 0.06

the number of input parameters. For this case the input parameters are the O vi $\lambda1032/\lambda1037$ intensity ratio, T_e, electron density, parallel kinetic temperature [$T_k(\|)$], and I_{disk}(O vi), which in turn gives the outflow velocity (e.g., Strachan et al. 2002).

Table 5 shows the range of possible O^{5+} outflow velocities, V_{out}, that are consistent with the range of uncertainties in the model inputs. For example the electron density, derived from the LASCO C2 pB data, is modeled with one-half and twice its nominal values. The T_e is varied from 0.7 to 1.3 MK, since there are no constraints provided by the ion intensities above 2 $R_\odot$. Finally, there were a range of values used for $T_k(\|)$ that characterize the kinetic temperatures along the radial direction (not observed). The values for $T_k(\|)$ range in value from a minimum equal to T_e and a maximum of $T_{k,O}$. The upper and lower limits to V_{out} in Table 5 represent the minimum and maximum results produced from all possible input parameter combinations.

8. DISCUSSION AND CONCLUSION

In § 2 it was determined that Str030428, Str030509, and Str030925 are all quiescent streamers. This conclusion was based on the lack of active regions located at the base of the streamers. However, the contributions from nearby active regions cannot be ruled out, such as the southern leg of Str030925 (see § 5). To facilitate the comparisons of the new results for the streamer plasma parameters with previously published results, we provide Tables 3–5. A brief description of the earlier published entries can be found in Paper I. All abundances are renormalized using the photospheric abundances of Grevesse & Sauval (1998) and for oxygen (Asplund et al. 2004), where applicable.

Quiescent streamers are typically associated with low T_e, since they do not form above active regions. The electron temperatures for Str030428 (1.82 MK), Str030509 (1.65 MK), and Str030925 (1.75 MK) at 1.75 $R_\odot$ do not fit this model, as these quiescent streamers have the highest values of the streamers listed in Table 3. These electron temperatures are similar to those for the active region streamer from Uzzo et al. (2004). One explanation for these high temperatures could be the result of a high degree of complexity for the magnetic field within these streamers. A complex magnetic structure is theoretically predisposed to having a large number of reconnection events that could heat the streamer plasma. It should be noted that the degree of magnetic field complexity needed to account for this is unknown, and once again none of the streamers formed over active regions. Another reason for the high values of T_e could be the presence of higher temperature plasma outside the streamer along the LOS.

The electron density at 1.75 $R_\odot$ for the three new streamers is consistent with the results listed in Table 3 from Bemporad et al. (2003) for an active region streamer. The remaining entries for the electron density in Table 3 differ from the new results by up to an order of magnitude. Much of the difference between Parenti et al. (2000) and the results for the new streamers can be traced to the values used for I_{1032}(disk). Parenti et al. (2000) used a static value of 305 ergs cm^{-2} s^{-1} sr^{-1}. However, for the present study, we determined I_{1032}(disk) for each streamer based on UVCS observations that are case specific. After the data from Str030428 were analyzed using the DAS version 4.0 calibrations, the value of η increased from 0.3 to 0.62. Since the electron density derived from UVCS data (eq. [3] in Paper I) is proportional to I_{1032}(disk), the change corresponds to an increase of the electron density from 1.84×10^7 to 3.22×10^7 cm^{-3}. At higher heights the electron densities were derived from the LASCO C2 pB measurements. Table 5 shows that the derived densities at 2.5, 3.0, 4.0, and 5.0 $R_\odot$ for the streamers in the present study are similar to the values found by Strachan et al. (2002) for an equatorial solar minimum streamer. All four streamers have a similar change in density with radial height.

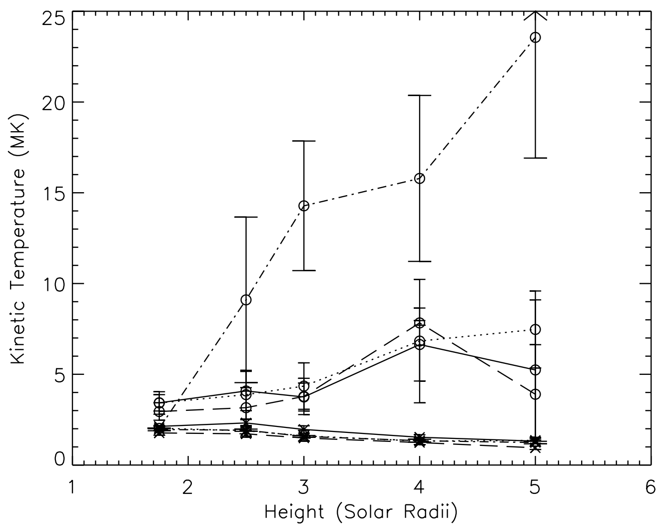

FIG. 11.—Kinetic temperature (MK) vs. height ($R_\odot$) for Str030428 (*solid lines*), Str030509 (*dashed lines*), Str030925 (*dotted lines*), and Strachan et al. (2002, *dash-dotted lines*) for O^{5+} ions (*circles*) and protons (*crosses*).

A significant improvement in the agreement between oxygen abundances derived from the collisional intensities and those derived from the radiative intensities were found using the techniques outlined in §§ 3 and 5. Table 3 provides oxygen abundances derived from both intensity components as published by Raymond et al. (1997), Parenti et al. (2000), and Marocchi et al. (2001). From these earlier studies, the ratio of the abundances using the two methods (i.e., radiative over the collisional) varied from 1.4 to 3.7. By comparison the abundance ratios for the 2003 streamers vary from 0.8 to 1.5. As mentioned earlier the value of η for Str030428 nearly doubled from the Paper I results. Despite the increase in the derived oxygen and hydrogen disk intensities, there are essentially no changes to the oxygen abundances.

Another interesting feature of the three streamers presented here is that they do not have the expected abundance-depleted cores. Normally, quiescent streamers have depleted cores and active region streamers do not (Raymond et al. 1997). There are a number of plausible reasons for the lack of an abundance-depleted core. For example, it is possible that a large number of reconnection events, as implied by the higher T_e, could allow trapped material from lower heights in the streamer base to escape and replenish the streamer core. A counter example, however, is found by Uzzo et al. (2004), who reported on an active region streamer with both a high T_e and an abundance-depleted core. Another factor to consider is the orientation of the closed magnetic field lines

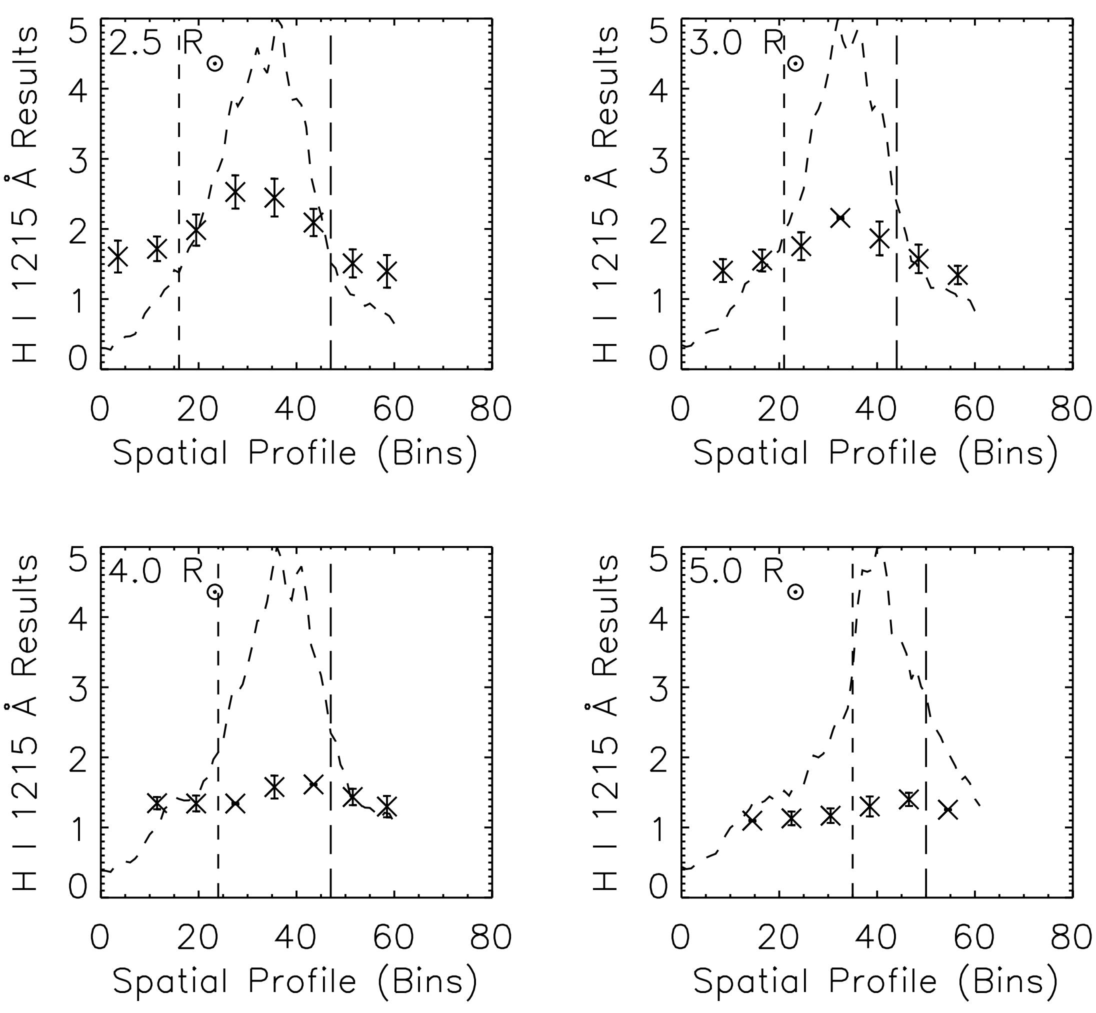

FIG. 12.—Composite of four plots for the upper four heights of Str030428, with each height identified in the upper left corner. For each graph the H I Lyα intensity (*dashed lines*) and proton kinetic temperature (*crosses*) in MK vs. spatial profiles along UVCS FOV (1 bin = 35″) are plotted. The Lyα intensity curves are each normalized to a peak intensity of 5 using 8.593×10^9, 3.595×10^9, 1.035×10^9, and 4.327×10^8 for 2.5–5.0 $R_\odot$, respectively.

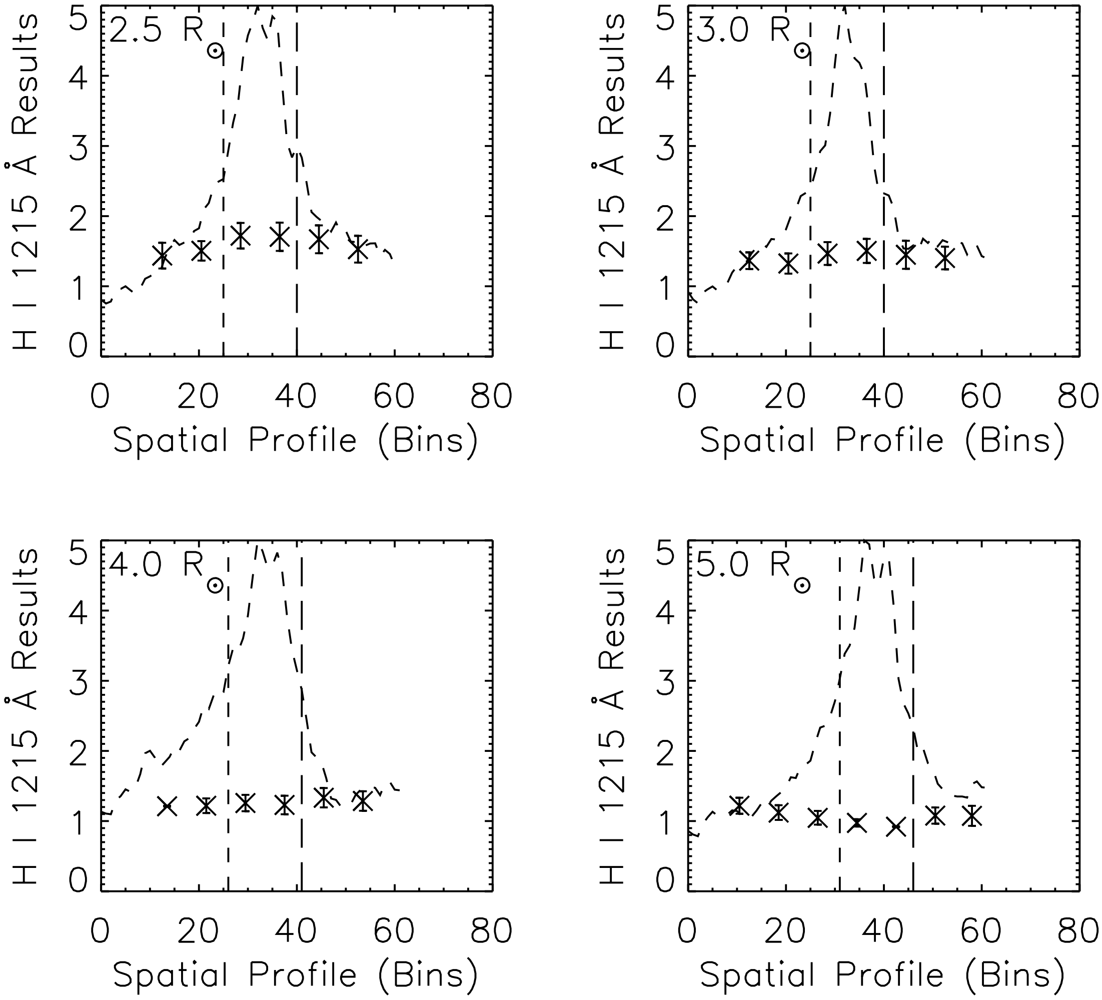

Fig. 13.—Same as Fig. 12 for Str030509, except using 9.937×10^9, 4.311×10^9, 1.073×10^9, and 5.239×10^8 for the normalized intensity profiles of 2.5–5.0 $R_\odot$, respectively.

that make up the core. If multiple loops overlap along the LOS, projection effects could explain the lack of a depleted core. Strachan et al. (2002) showed an order-of-magnitude increase in $T_{k,\mathrm{O}}$ at the legs compared to core. Since the intensity profile from the Strachan et al. (2002) streamer indicated the presence of a depleted core, it is possible that this reduced $T_{k,\mathrm{O}}$ at the same structure are connected. The $T_{k,\mathrm{O}}$ values for all three streamers at 1.75 $R_\odot$, shown in Figures 5–7, lack this order-of-magnitude decrease. The proposed abundance–kinetic temperature correlation is therefore consistent with the current results, since no abundance depletion and no suppressed values for $T_{k,\mathrm{O}}$ at the cores are detected. The kinetic temperature spatial profile is further explored below.

In Table 4 the photospheric normalized absolute elemental abundances of oxygen, sulfur, argon, and iron from previous studies are provided for comparison with the three streamers from 2003. When these three sets of four abundances are compared to the previous results, we find they have significantly higher values compared to the quiescent cores (QCs). The abundances derived for O, S, Ar, and Fe from the three streamers reported here match reasonably well with active region (AR) and quiescent leg (QL) values reported in past publications. In several cases the AR abundances are similar to those found in QLs. It should also be noted that the abundances for the AR streamers from Table 4 fall within the range of values between the active region leg (AL) and core (AC) reported in Uzzo et al. (2004). This implies the possibility that when sampling over the entire streamer for the AR cases the results reflect the presence of a leg and core blend along the LOS. Therefore, the same phenomenon may be present for the three streamers in the current study. These three streamers may in fact be a composite of blend of QL and QC structures sampled along the LOS based on the these abundance results.

The FIP effect, where the high-FIP elements are depleted while the low-FIP elements are enhanced relative to their photospheric values, is present in all three streamers. A FIP bias of $\sim$4 was found using the iron-to-oxygen abundance ratio. This matches the values typically found for the slow solar wind from in situ measurements. According to a streamer model presented by Bemporad et al. (2003), the FIP effect occurs at the chromospheric height. At higher heights gravitational settling, or some other phenomenon, reduces the abundances of all elements within the streamer. As a result the FIP effect manifestation is preserved. The present results are consistent with this model.

The perpendicular kinetic temperatures for the protons (*crosses*) and the O^{5+} ions (*circles*) from Table 5 are plotted in Figure 11 for Str030428 (*solid lines*), Str030509 (*dashed lines*), Str030925 (*dotted lines*), and Strachan et al. (2002, *dash-dotted lines*) as a function of height. The error bars for the $T_{k,p}$ from this study are too small to discern in Figure 11. The $T_{k,p}$ for all four of the streamers shows a small decrease with height between 1.75 and 5.0 $R_\odot$. This decrease averages 0.82 MK for the 2003 streamers and 0.72 MK for the Strachan et al. (2002) streamer. Contrary to the $T_{k,p}$, the $T_{k,\mathrm{O}}$ increases with height and there is an obvious

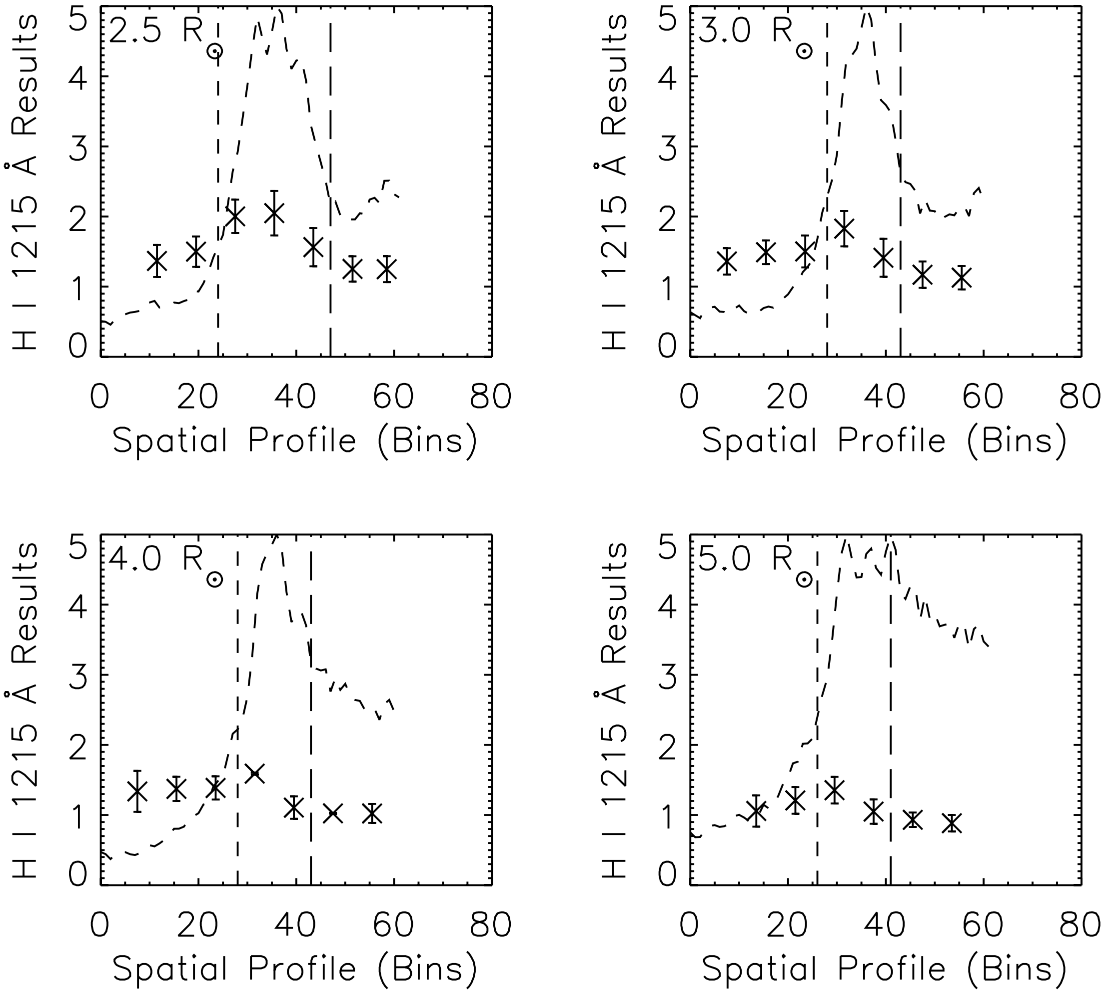

FIG. 14.—Same as Fig. 12 for Str030925, except using 8.060×10^9, 3.646×10^9, 9.601×10^8, and 3.322×10^8 for the normalized intensity profiles of 2.5–5.0 $R_\odot$, respectively.

preferential heating of the O^{5+} ions at all heights in the streamers. However, the magnitude of the $T_{k,\mathrm{O}}$ for the three 2003 streamers reported here are much lower in contrast to the Strachan et al. (2002) streamer. The perpendicular kinetic temperatures can be thought of as having a thermal and a nonthermal component. By assuming that the thermal component of the proton perpendicular kinetic temperature $T_{\mathrm{th},p}$ is the same as the T_e at 1.75 $R_\odot$, the nonthermal components for Str030428, Str030509, and Str030925 are 0.31, 0.12, and 0.28 MK, respectively.

Next we discuss the latitudinal variation in the streamer plasma parameters for different heights. As previously mentioned at 1.75 $R_\odot$ the $T_{k,\mathrm{O}}$ and $T_{k,p}$ are presented as a function of latitude for the three streamers in Figures 5–7, respectively. Quad plots of the latitudinal profiles for $T_{k,p}$ at four different heights (2.5–5.0 $R_\odot$) are shown in Figures 12–14, respectively, for each of the three streamers. The $T_{k,\mathrm{O}}$ for Str030428 and particularly Str030509 indicates a possible decrease in value toward the center of the streamer. However, the degree of change in these two cases, which are less than a factor of 2, is small compared to the order-of-magnitude change found in Strachan et al. (2002). For the Str030925 case the values appear to lack a coherent pattern, although the maximum change is still under a factor of 2. One possible reason for this random result is the presence of the second structure, as discussed earlier. Another reason is that the statistical errors are larger for this streamer due to its lower O VI doublet count rates. The spectral profile measurements for this streamer occurred at the end of the observation. By that time, the streamer had started to rotate behind the limb. As a result, the observation alignment was hampered and the time dedicated to this component was less compared to the first two streamers.

The $T_{k,p}$ at 1.75 $R_\odot$ indicates a trend where the values within the streamer are slightly elevated compared to outside. This tendency decreases with height. For Str030428 (Fig. 12) and Str030925 (Fig. 14) the elevated values toward the streamer core are present at 2.5 and 3.0 $R_\odot$. By 4.0 $R_\odot$ the temperatures have essentially leveled out across the FOV. For Str030509 (Fig. 13) the higher core temperatures are present at 1.75 $R_\odot$ and possibly at 2.5 $R_\odot$. The values outside the streamers at the lower heights are approximately the same as those found across the FOV at the upper heights. This could map out the streamer morphology and indicate the height of the cusp. The model depicted in Figure 1 shows the open magnetic fields of the legs flanking the streamer core, which then come together above the cusp and travel radially outward as the stalk. In this scenario the kinetic temperature along the open field lines could be isothermal within the short distance considered. Under this hypothesis the cusps for Str030428 would be between 3.0 and 4.0 $R_\odot$, below 3.0 $R_\odot$ for Str030509, and just above 3.0 $R_\odot$ for Str030925. These are of course rough approximations, and the maximum change in values across the FOV for any case are under a factor of 2. It should also be noted that the plasma located at the edge of the UVCS FOV is at a greater heliocentric height compared to the plasma located toward the center. This could lead to a decrease in the derived $T_{k,p}$ with increased distance from the streamer axis. However, the confidence in the proton results is significantly higher than the oxygen results. An ideal target for investigating this phenomenon would be a streamer with a well-defined abundance-depleted core. In theory this would provide a greater change in kinetic temperatures across the streamer. It is interesting to note that at 5.0 $R_{\odot}$ for Str030509 there is a slight decrease in the $T_{k,p}$ within the streamer. Since the analysis suggests that the cusp for this streamer is lower compared to the other two, there may be a connection. Further investigation on the possible connection of magnetic field morphology and kinetic temperatures is certainly warranted.

Outflow velocities for O^{5+} were calculated for the three new streamers using the latest version of the DAS and taking into account the range of uncertainties in all of the model parameters. The outflow velocities were similar to the values derived at the same heights for an equatorial streamer at solar minimum (Strachan et al. 2002). Significant outflow occurs at 4 $R_{\odot}$ or above. At 5 $R_{\odot}$ the outflow velocities for the three streamers reported here vary from 102 to 176 km s^{-1}; this is slightly higher than the mean value reported at this height by Strachan et al. (2002).

The similarity in the values for the FIP effect and elemental abundances detected in the slow solar wind to those observed in coronal streamers suggests that streamers are a source for slow-speed wind streams. The low outflow speeds in streamers, compared to the speeds measured in coronal holes at the same heights, also supports this idea. The potential connection between the $T_{k,p}$ results and the streamer morphology reported here agree with this hypothesis. However, the amount that streamers contribute to the slow solar wind cannot be determined from these results alone. Additional investigations of streamers as well as other potential sources (examples include the boundaries of high-latitude coronal hole and equatorial coronal holes) are required in combination with advancements in heliospheric transport models. Equatorial studies at solar minimum of remote streamer observations and corresponding in situ measurements of the slow solar wind will certainly advance this research.

SOHO is a project of international collaboration between ESA and NASA. This work was performed under NASA grant NNG 06GI88G to the Smithsonian Astrophysical Observatory.

REFERENCES

Asplund, M., Grevesse, N., Sauval, A. J., Allendem, P. C., & Kiselman, D. 2004, A&A, 417, 751
Bemporad, A., et al. 2003, ApJ, 593, 1146
Binello, A. M., Landi, E., Mason, H. E., Storey, P. J., & Brosius, J. W. 2001, A&A, 370, 1071
Brueckner, R. A., et al. 1995, Sol. Phys., 162, 357
Delaboudinière, J.-P., et al. 1995, Sol. Phys., 162, 291
Dere, K. P., Landi, E., Mason, H. E., Fossi, B. C., & Young, P. R. 1997, A&AS, 125, 149
Feldman, U., Schühle, U., Widing, K. G., & Laming, J. M. 1998, ApJ, 505, 999
Gardner, L. D., Atkins, N., Fineschi, S., Smith, P. L., Kohl, J. L., Maccari, L., & Romoli, M. 2000, Proc. SPIE, 4139, 362
Gardner, L. D., et al. 1996, Proc. SPIE, 2831, 2
Geiss, J. 1982, Space Sci. Rev., 33, 201
Grevesse, N., & Sauval, A. J. 1998, Space Sci. Rev., 85, 161
Habbal, S. R., Woo, R., Fineschi, S., O'Neal, R., Kohl, J., Noci, G., & Korendyke, C. 1997, ApJ, 489, L103
Ko, Y.-K., Raymond, J. C., Li, J., Ciaravella, A., Michels, J., Fineschi, S., & Wu, R. 2002, ApJ, 578, 979
Kohl, J. L., et al. 1995, Sol. Phys., 162, 313
———. 1997, Sol. Phys., 175, 613
Laming, J., & Feldman, U. 1999, ApJ, 527, 461
Landi, E., & Phillips, K. 2005, ApJS, 160, 286
Li, J., Raymond, J. C., Acton, L. W., Kohl, J. L., Romoli, M., Noci, G., & Naletto, G. 1998, ApJ, 506, 431
Marocchi, D., Antonucci, E., & Giordano, S. 2001, Ann. Geophys., 19, 135
Mazzotta, P., Mazzitelli, G., Colafrancesco, S., & Vittorio, N. 1998, A&AS, 133, 403
Noci, G., Kohl, J. L., & Withbroe, G. L. 1987, ApJ, 315, 706
Parenti, S., Bromage, B. J. I., Poletto, G., Noci, G., Raymond, J. C., & Bromage, G. E. 2000, A&A, 363, 800
Pernechele, C., Naletto, G., Nicolosi, P., Poletto, L., & Tondello, G. 1995, Proc. SPIE, 2517, 79
Raymond, J. C. 1999, Space Sci. Rev., 87, 55
Raymond, J. C., Ciaravella, A., Dobrzycka, D., Strachan, L., Ko, Y.-K., & Uzzo, M. 2003, ApJ, 597, 1106
Raymond, J. C., et al. 1997, Sol. Phys., 175, 645
———. 2001, in AIP Conf. Proc. 598, Joint *SOHO/ACE* Workshop: Solar and Galactic Composition, ed. R. F. Wimmer-Schweingruber (Melville: AIP), 49
Scherrer, P. H., et al. 1995, Sol. Phys., 162, 129
Sheeley, N. R., et al. 1997, ApJ, 484, 472
Strachan, L., Panasyuk, A. V., Dobrzycka, D., Kohl, J. L., Noci, G., Gibson, S., & Biesecker, D. A. 2000, J. Geophys. Res., 105, 2345
Strachan, L., Suleiman, R., Panasyuk, A. V., Biesecker, D. A., & Kohl, J. L. 2002, ApJ, 571, 1008
Uzzo, M., Ko, Y.-K., & Raymond, J. C. 2004, ApJ, 603, 760
Uzzo, M., Ko, Y.-K., Raymond, J. C., Wurz, P., & Ipavich, F. M. 2003, ApJ, 585, 1062
Uzzo, M., Strachan, L., Vourlidas, A., Ko, Y.-K., & Raymond, J. C. 2006, ApJ, 645, 720 (Paper I)
Vásquez, A. M., van Ballegooijen, A. A., & Raymond, J. C. 2003, ApJ, 598, 1361
Vernazza, J. E., & Reeves, E. M. 1978, ApJS, 37, 485
Wang, Y.-M., et al. 1998, ApJ, 498, L165
Withbroe, G. L., Kohl, J. L., Weiser, H., & Munro, R. H. 1982, Space Sci. Rev., 33, 17
Woo, R., & Martin, J. 1997, Geophys. Res. Lett., 24, 2535
Zangrilli, L., Nicolosi, P., Poletto, G., Noci, G., Romoli, M., & Kohl, J. L. 1999, A&A, 342, 592